On the iron content of Mn-Ni-Si-rich clusters that form in reactor pressure vessel steels during exposure to neutron irradiation

Benjamin M Jenkins, Aidar Zakirov, François Vurpillot, Auriane Etienne, Cristelle Pareige, Philippe Pareige, Bertrand Radiguet

Acta Materialia 281 (2024) 120384

Contents lists available at ScienceDirect

Acta Materialia

journal homepage: www.elsevier.com/locate/actamat

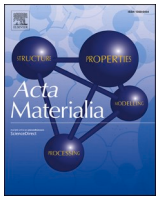

Full length article

On the iron content of Mn-Ni-Si-rich clusters that form in reactor pressure vessel steels during exposure to neutron irradiation

Benjamin M. Jenkins *, Aidar Zakirov *, François Vurpillot, Auriane Etienne, Cristelle Pareige, Philippe Pareige, Bertrand Radiguet

Univ Rouen Normandie, CNRS, INSA Rouen Normandie, Groupe de Physique des Matériaux UMR 6634, F-76000 Rouen, France

ARTICLE INFO

Keywords:
Reactor pressure vessel steels
Atom probe tomography (APT)
Irradiation embrittlement
Modelling
Solute clustering

ABSTRACT

Solute cluster formation during service is the primary cause of embrittlement in reactor pressure vessel (RPV) steels. Atom probe tomography (APT) has consistently shown that the solute clusters are enriched in Cu, P, Mn, Ni, and Si compared to the matrix. However, there is pronounced disagreement within the literature as to the Fe content of the solute clusters in low-Cu RPV steels; some authors report Fe contents in excess of 80 at.% whilst others attribute all measured Fe in the clusters to aberrations from APT and report Fe-free features. This discrepancy has profound implications for determining whether cluster formation is radiation-induced or radiation-enhanced.

In this article, we perform a systematic analysis of the published literature to demonstrate the variance present in the measured Fe content of solute clusters characterised by APT. We investigate potential explanatory variables for this variation and discuss the difficulties in performing statistical analyses on these data. To determine the impact of APT aberrations on the measured Fe content of solute clusters, we combine results from: simulations that account for the limited spatial precision in APT; models that predict ion trajectories in the presence of non-uniform electrostatic fields; and experimental data.

Our results show that APT aberrations can introduce large amounts of artificial Fe into solute clusters, especially at the small sizes (radius <1.5 nm) typically observed in RPV steels. We also show, however, that some of the variance in Fe content in the literature may be explained by real differences in the clusters' Fe contents.

1. Introduction

Reactor pressure vessel (RPV) steels are known to embrittle during service, primarily as a result of the formation of solute clusters. These features have been extensively characterised using a range of techniques including small angle neutron scattering (SANS), small angle X-ray scattering (SAXS), and transmission electron microscopy (TEM) [1–10]. However, due to its ability to directly provide compositional information on small features, atom probe tomography (APT) has emerged as the leading method with which to study clusters in RPV steels [11–13].

Previous APT studies show that clusters in older, Cu-containing, RPV steels are comprised mainly of Cu [14] but also contain other solutes, particularly Mn, Ni, and Si [15,16]. The composition of these features has been shown to vary as a function of size [15] and as a function of distance from the interface between the cluster and the matrix [14,17]. In low-Cu alloys, features enriched in Mn, Ni, and Si are responsible for hardening [18,19]. The exact composition of these features is a matter of lively debate within the community; the primary source of disagreement being what the true iron content of the clusters is.

Some researchers state that the majority of the Fe measured within the clusters by APT is the result of experimental aberrations. As a result, Fe is excluded from size, volume fraction, and compositional analyses, and Fe contents of 0 at.% are reported [20–22]. Although infrequently communicated, these studies tend to experimentally measure Fe contents of between 40 at. % and 60 at. % within the clusters [23–25]. Authors typically justify their decision to exclude Fe from their results by attributing the measured Fe within clusters to trajectory overlaps, which occur in APT as a result of the local magnification of ions due to the solute clusters having a lower evaporation field than the surrounding matrix [26]. The assumption that the solute clusters are lower field than the matrix and subject to appreciable local magnification is based upon the observation of increased measured atomic density within the

* Corresponding authors.
E-mail addresses: benjamin.jenkins@univ-rouen.fr (B.M. Jenkins), aidar.zakirov0@univ-rouen.fr (A. Zakirov).

https://doi.org/10.1016/j.actamat.2024.120384
Received 17 July 2024; Received in revised form 6 September 2024; Accepted 6 September 2024
Available online 7 September 2024

clusters [24] and due to the decreasing concentration of Fe towards the centre of the clusters [23]. Further evidence that the solute clusters contain limited amounts of Fe come from studies where complementary techniques, such as STEM-EDS (Scanning Transmission Electron Microscopy – Energy Dispersive X-ray Spectroscopy), were used to estimate that clusters contain around 6 at.% Fe [4].

In contrast, multiple other articles on RPV alloys report clusters containing up to 80 at.% and even 92 at.% Fe [27–30]. The authors of these studies believe that their experimental measurements of cluster composition are either not influenced by APT aberrations, such as local magnification and limited spatial precision [31,32], or they assume that their measurements are performed sufficiently far away from the interface between the matrix and cluster that these effects are considered negligible.

There is, therefore, a range of reported Fe contents between 0 at.% and 92 at. % in the RPV literature. This large discrepancy has profound effects on the interpretation of experimental data and on understanding the underlying mechanisms that control solute cluster formation in RPV steels. For example, authors often use the presence of Fe within the clusters to support the hypothesis that the clusters are non-thermodynamically stable phases and are therefore radiation induced [33], whilst others interpret the clusters to be thermodynamically stable phases that are formed by radiation enhanced diffusion and contain no Fe [18,34]. Additionally, the inclusion or exclusion of Fe within the clusters also impacts the determination of feature size and volume fraction within alloys. Since mechanical property shifts are known to be related to the volume fraction and size of dislocation barriers [35], the creation and validation of models that predict mechanical property shifts during service [36], particularly at extended lifetimes, will be adversely affected by erroneous measurements of these cluster characteristics.

There is, therefore, a pressing need to determine how accurately APT is capable of measuring the Fe content of the solute clusters that form in RPV steels. In turn, this will permit ascertainment as to whether the range of 0 at.% and 92 at. % in the literature is representative of the true range of cluster Fe contents, or if the range is likely to be smaller. Another outstanding question is what are the primary causes for such large differences in the reported Fe content of clusters. The use of different cluster search methodology is often cited as a potential source of divergence [37,38], but there are multiple other explanatory variables that change between published studies. Some examples include: alloys of different nominal compositions (e.g. very high solute contents [18,24] cf. much lower solute contents [27,39]); alloys that have been irradiated under very different conditions (e.g. [19] cf. [40]); characterisation of clusters with very different sizes that are unlikely to experience the same level of APT experimental aberrations (e.g. [41] cf. [42]). In this article we attempt to address these pending uncertainties as to the nature of Mn-Ni-Si-rich features that form in RPV steels.

Firstly, we perform a systematic review of the published literature on neutron-irradiated RPV steels that have been characterised using APT. After extracting quantitative data from the literature, we demonstrate the degree of variation between studies and propose potential explanations for the variance. By then applying different cluster search algorithms to experimental data we show that this alone is unlikely to be responsible for the wide variation observed in the literature. We then investigate how accurately APT can be expected to characterise the Fe content of solute clusters in RPV steels by performing simulations to study the role of imperfect spatial precision on compositional measurements. We also explore the possible role of trajectory aberrations by modelling the trajectories of ions after field evaporation in the presence of a variety of non-uniform evaporation fields.

Our results show that significant amounts of Fe can be introduced into solute cluster measurements as a result of APT aberrations, especially at the sizes typically observed in RPV steels, but that at least some of the deviation in Fe contents within the literature is likely to be due to the solute clusters themselves being different in nature and containing slightly different Fe contents. This work represents an important contribution to the understanding of the nature of solute clusters that form in RPV steels during service; this will have an impact on assessments as to the clusters' formation mechanisms and, hence, on models that predict changes in mechanical properties during service.

2. Experimental methods

2.1. Systematic review of literature

A systematic review of the literature was conducted. Identification of relevant articles was achieved by using Elsevier's Scopus abstract and citation database in April 2024. The following search terms and Boolean operators were used: "atom probe" AND "neutron irradiation" AND "reactor pressure vessel steel". A total of 51 documents were returned from this search of which five articles were inaccessible and one was unavailable in English. Therefore, 45 articles were screened to determine their suitability for inclusion; three of these were excluded as they either concentrated on ion irradiation studies or non-RPV materials.

Data were extracted from the remaining 42 articles. Of these 42 articles, 31 reported the composition of solute clusters measured by APT. The nominal Fe, Mn, Ni, Si, and Cu contents in each alloy were recorded along with neutron irradiation fluence, flux, and temperature. The APT instrument used, the cluster search method employed, the measured cluster number density, volume fraction, and radius were also extracted. The measured cluster contents of Fe, Mn, Ni, Si, and Cu were also included, along with the Fe content that the authors believed was present in the clusters (if this differed from the raw measured value).

2.2 APT experiments

2.2.1 Analysis of clusters in neutron-irradiated steels

APT data from two neutron-irradiated steels were analysed using both the Iso-Position and Maximum Separation cluster search algorithms. One of the steels (HN) had a high solute content, whilst another had much lower Ni levels (LN). The compositions of the steels are presented in Table 1.

Alloy HN was irradiated to a fluence of 1.4×10^{24} n/m^2 at a flux of 3.6×10^{16} n/m^{2}s at 290 °C in the Advanced Test Reactor (ATR-2) experiment. Further details on its manufacturing route can be found in Ref. [24]. It was analysed on a LEAP 4000X HR in voltage pulsing mode at 55 K with a pulse frequency of 200 kHz and a pulse fraction of 20 %.

Neutron irradiation to a total fluence of 9.34×10^{23} n/m^2 was performed on alloy LN, provided by SCK CEN (Belgium), in the BR2 reactor at 290 °C. This irradiation was conducted in two campaigns, the first campaign used a neutron flux of 2.45×10^{17} n/m^{2}s to reach a fluence of 5.99×10^{23} n/m^2, whilst the second campaign attained an additional fluence of 3.35×10^{23} n/m^2 at a flux of 1.18×10^{17} n/m^{2}s. Further details on the irradiation conditions and manufacturing process for this alloy can be found in Ref. [43]. Alloy LN was analysed using a LEAP 4000X HR in voltage pulsing mode at 60 K with a pulse frequency of 200 kHz and a pulse fraction of 20 %.

Reconstructions for both alloys were performed using IVAS 3.8.0. Maximum Separation cluster searches [44] were conducted using IVAS 3.8.16 whilst the Iso-Position method [45] was implemented through the GPM_3DSAT Software (CNRS IDDN: IDDN.FR.001.430017.000.S.P.2020.000.10000). Edge clusters were manually identified and were not included in the size or compositional calculations that follow. Cluster radii, both including and excluding measured Fe, were calculated using the equivalent radius, assuming the atomic density of BCC Fe and a detection efficiency of 0.37.

Maximum Separation parameters were individually selected for each dataset to ensure that the identified solute clusters were statistically unlikely to be identified in a mass-randomised dataset; the applied parameters are presented in Table 2. The justification for using a larger D_{max} value for the LN dataset is that this alloy contained lower bulk

Table 1
Nominal composition of the steels used in this study.

Alloy	Cu (at.%)	Si (at.%)	Ni (at.%)	Mn (at.%)	P (at.%)	Cr (at.%)	Mo (at.%)	C (at.%)	Fe (at.%)
HN	0.04	0.37	3.11	1.90	0.01	0.10	0.27	0.87	Bal.
LN	0.04	0.49	0.67	1.77	0.02	0.00	0.30	0.94	Bal.

Table 2
Parameters used for Maximum Separation cluster searches in both alloys.

Alloy	Core Ions	D_{max} (nm)	Order (ions)	N_{min}	L (nm)	E (nm)
HN	P, Si, Mn, Ni	0.55	6	20	0.40	0.40
LN	P, Si, Mn, Ni	0.65	1	40	0.55	0.55

levels of core ions, and so these ions are likely to be separated by a greater distance in a mass-randomised dataset. The 29 Da peak (where Da represents the mass-to-charge ratio of an ion and is equivalent to atomic mass unit per Coulomb), which contains an overlap between $^{58}Fe^{2+}$ and $^{58}Ni^{2+}$, was assigned as Ni for the cluster searches since, based on natural isotopic abundances, over 90 % of this peak is expected to be Ni in alloy LN and more than 98 % of this peak would be Ni in alloy HN.

For the Iso-Position method, Mn, Ni (including the 29 Da peak), Si, P, and Cu were considered as core atoms. After atom filtering was performed using the concentration thresholds in Table 3; clusters were identified in the filtered volumes by linking any atoms spatially located within a specified atomic distance of one other. Equivalent cluster size was calculated after a "first erosion" step was performed and compositional calculations were carried out after "double erosion" was performed to leave only the cluster core.

An alternative measurement of cluster size was taken by performing a one-dimensional profile through the solute clusters; this profile was taken in the z-direction (parallel to the analysis direction) in each dataset. A compositional profile was then generated and the cluster diameter was determined to be the width at the half maximum of solute composition. The ratio of atomic density of the clusters was calculated by comparing the atomic density in the matrix to that within the clusters from the one-dimensional profile.

2.2.2. Estimation of lateral precision

As a microscopy technique, APT is defined by spatial metrological parameters. Note that we will not use the term "spatial resolution", which is defined as the minimum feature that can be observed by a microscope, when referring to the reconstructed spatial location of individual ions/atoms and will instead refer to "spatial precision". Readers should note that "spatial resolution" can, however, be used in APT when referring to composition maps or density maps. Spatial resolution in APT is valid when measuring features composed of a large number of atoms such as segregation thickness, an interface, or a precipitate for instance.

The rationale for this is that the position of each atom in APT is represented by three floating values (x, y, z) and there is no pixel size, whereas the spatial resolution of a classical microscope operating under ideal conditions is limited by the size of the pixels on the camera. In APT, each measured atom position is the result of a single experiment. It therefore makes sense to refer to its accuracy and precision, where the spatial precision of an experiment can be defined as the spatial dispersion corresponding to the measurement of a position in a single experiment. It can be estimated by repeating a large number of experiments. The distribution of the values around the average value gives an estimate of the precision. As a result, the use of "spatial resolution" to refer to a single atom's position is awkward; we will refer to "spatial precision" instead.

Previously, multiple authors have demonstrated that worse lateral precision in APT experiments will increase the likelihood of matrix atoms being misidentified as belonging to solute clusters [46–48]. Therefore, precise knowledge of the spatial precision of APT measurements on instruments typically used to analyse RPV steels is of paramount importance and experiments were performed on a range of instruments under a variety of analysis conditions. Where appropriate in the text, the specifics of each experiment are reported. The lateral precision was determined in the vicinity of crystallographic poles in each dataset using the method presented by Vurpillot et al. [49,50]. It is important to stress that the precision (σ) that is measured by this Fourier measurement method is indicative of the precision in one of the x or y co-ordinates. We assume that the precision in the orthogonal x or y co-ordinate is similar and, when performing simulations, it is therefore important to independently apply an uncertainty of σ to both the x and y co-ordinates of individual atom positions. In previous simulations within the literature it is not always clear if the uncertainty in atomic locations has been applied independently to the x and y co-ordinates. For example, in Ref. [48] the limited spatial precision of atomic locations in APT was attributed to the distance, L, between the exact and measured position (where $L = \sqrt{\Delta x^2 + \Delta y^2}$). It is important to note that this is not representative of what is measured using the Fourier measurement method; this would lead to much smaller displacements in the x and y co-ordinates of the atoms in the simulations in Ref. [48] and would result in a large underestimation of the degree of matrix mixing into the solute clusters.

Table 3
Parameters used for Iso-Position cluster searches in both alloys.

Alloy	Concentration Threshold (at.%)	Atomic Distance (nm)	N_{min}	D_{Ero1} (nm)	D_{Ero2} (nm)
HN	12	0.40	10	0.45 - 0.72	0.90 - 1.56
LN	7	0.40	15	0.33 - 0.45	0.63 - 0.84

3. Calculation/simulations

3.1. Simulations of limited spatial precision in APT

To investigate the relationship between cluster size, spatial precision, and the amount of matrix Fe that could be incorporated into the solute clusters and detected by different cluster search algorithms, a series of simulations were performed. These simulations permitted a wide-range of cluster sizes, spatial precisions, and original Fe contents to be explored. The simulations were conducted using R version 4.2.1 [51].

To represent α-Fe, a 16 nm x 16 nm x 16 nm volume was created with a body-centred cubic (BCC) structure and a lattice parameter of 0.2866 nm. A cluster was then placed at the centre of this volume before 48% of the atoms were randomly removed from the entire volume to represent the imperfect detection efficiency of LEAP 5000 XR instruments. All remaining atoms were subjected to independent random perturbations in their x and y co-ordinates based on a Gaussian distribution with a mean (μ) = 0 and a standard deviation (σ) = Lateral Precision. This process is shown in Fig. 1 for a single simulation that contained a cluster of radius 1 nm and a spatial positioning accuracy of σ = 0.6 nm.

Cluster radii were varied between 0.5 nm and 3.0 nm in step sizes of 0.05 nm, whilst lateral precision was investigated between 0 nm (perfect

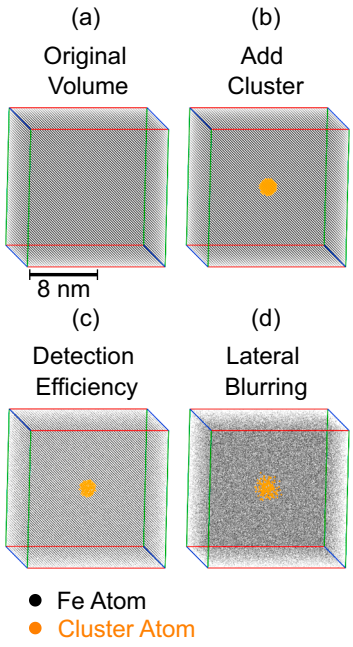

Fig. 1. Diagram demonstrating the workflow for the simulations to investigate the impact of the limited spatial precision of APT experiments. In this example, (b) the cluster originally contains 0 at.% Fe and has a radius of 1 nm. (c) A detection efficiency of 0.52 is accounted for, then (d) spatial blurring is applied to represent a lateral precision of $\sigma = 0.6$ nm.

precision) and 1.5 nm with a step size of 0.05 nm. A range of original Fe cluster contents, similar to those reported in the literature, were tested; original Fe contents of 0 at.% to 80 at.% were tested at step sizes of 20 at. %.

The Fe content of the clusters was then measured. Whilst it would have been desirable to use both the Maximum Separation and Iso-Position methods for this analysis, it was not possible due to the large number of simulated volumes (7,905). This, combined with the fact that both methods require decision making and parameter selection by the operator analysing the data, meant that analyses would have taken a prohibitively large amount of time. Whilst implementation of the maximum separation method can be scripted using software such as Ref. [52], the cluster search parameters (D_{max}, Order, N_{min}, L, and E) must be predefined by the user. Since appropriate values for these parameters, particularly D_{max}, are likely to change as lateral precision and original Fe content of the cluster varies, they would have to be manually tuned/optimised for each simulation. Meanwhile, the Iso-Position method is not currently automated and requires significant user input, particularly during the erosion steps.

As a result, the composition of the clusters was determined in two ways that we believe approximate the Maximum Separation and Iso-Position methods. The first method, which we consider a surrogate for Maximum Separation, simply calculated the composition using all atoms located in the original cluster volume after the spatial blurring step. The second method, which is considered representative of the "double erosion" method commonly implemented to determine composition by users of the Iso-Position method, only considered atoms within 0.8 nm of the original cluster centre (unless the original cluster radius was less than 0.8 nm, where the whole original cluster volume was considered). Whilst there are limitations associated with this approach that may affect the accuracy of the absolute values reported, the authors believe that general trends will not be adversely impacted.

3.2. APT evaporation trajectory simulations

As well as non-perfect spatial positioning due to processes such as atomic roll up [53] or surface diffusion [54], atoms that are originally in the matrix of the material can be detected in solute clusters in APT data as a result of trajectory aberrations [26,55,56]. Whilst it is assumed in APT reconstruction algorithms that the tip is hemispherical in shape, the presence of phases with evaporation fields that are dissimilar to the matrix can lead to local changes in the curvature of the tip. These changes in curvature affect the electrostatic field distribution around the tip, which in turn impacts the trajectory of ions that evaporate from the surface. In the case of low-field phases there will be a local flattening of the surface and a decrease in the curvature of the specimen, meaning that ions from the matrix can be projected into the same area of the detector where only cluster atoms would expect to be detected in the case of uniform evaporation.

To investigate how this phenomenon, combined with limited precision in spatial positioning, may impact the accuracy of APT measurements of the Fe content of solute clusters in RPV steels, computational simulations were performed. The simulations are based on the model described in [57,58].

In this model, a critical parameter is the selection of the assigned evaporation field of the secondary phase compared to the evaporation field of the matrix (F_{Matrix}). Since the evaporation field of the Mn-Ni-Si-rich features that are characterised in the literature is unknown, estimates were made using experimental data from alloy HN. The charge-state-ratio (CSR) of Cu^{+}:Cu^{++} within the clusters was compared to that within the matrix. In the clusters the CSR of Cu^{+}:Cu^{++} was around 1:3, whilst in the matrix all detected Cu was in the Cu^{++} charge state. The use of Kingham curves [59] for Cu enabled the field within the clusters ($F_{Cluster}$) to be estimated as being between 0.45 x F_{Matrix} and 0.93 x F_{Matrix}.

Initial simulations showed that clusters that had evaporation fields below 0.70 to 0.80 x F_{Matrix} experienced two simultaneous phenomena. Firstly, atoms from the clusters preferentially field evaporated with respect to matrix atoms, which tended to reduce the reconstructed depth axis dimension of the particle; this has been shown previously in the case of very low evaporation field clusters [60]. Secondly, the negative curvature of the surface in the vicinity of low-field clusters could induce negative magnification and ion crossing between the sample and the detector, which in-turn led to the low-field features appearing oblate in shape (dimensions elongated in the x-y plane), as also observed in [55,61]. The $F_{Cluster}$ value at which this cross-over occurs is dependent on the ratio of the cluster radius to the radius of the APT tip [61]; for the cluster radii and tip radius used in this study, this crossover was determined to occur below 0.80 x F_{Matrix}. Since a pronounced oblate shape in the x-y plane is not usually observed experimentally for clusters in RPV steels, the authors assume that evaporation field of Mn-Ni-Si-rich features that are present in RPV steels have an evaporation field between 0.80 x F_{Matrix} and 0.95 x F_{Matrix} and these values were used in the ensuing simulations.

A tip with α-Fe crystal structure and a radius 26 nm underwent simulated field evaporation (Fig. 2(a)). The predicted trajectory for each ion and its impact position on a detector were calculated. The tip contained 16 clusters, each with a composition representative of the Fe_x-$Solute_{100-x}$, where the solute was in the ratio 6Mn:17Ni:7Si; this solute ratio was chosen since it is reflects that which is expected for the G-Phase [62]. Four $F_{Cluster}$ values were investigated in each simulation, with four clusters each having $F_{Cluster}$ values of 0.80 x F_{Matrix}, 0.85 x F_{Matrix}, 0.90 x F_{Matrix}, and 0.95 x F_{Matrix}. Simulations were performed for clusters of initial radii of 1 nm and 2 nm. The tip radius and cluster radii were selected to be representative of those typically studied in the RPV literature, although the tip radius used in these simulations likely represents the lower end of the size of samples typically analysed experimentally. The clusters were located at symmetrical positions in the tip such that they would experience equivalent local electrostatic field environments (Fig. 2(c)). Simulations were performed for clusters that contained 0 at.%, 25 at.%, 50 at.%, and 75 at.% Fe.

After the simulated field evaporation had taken place, the data were

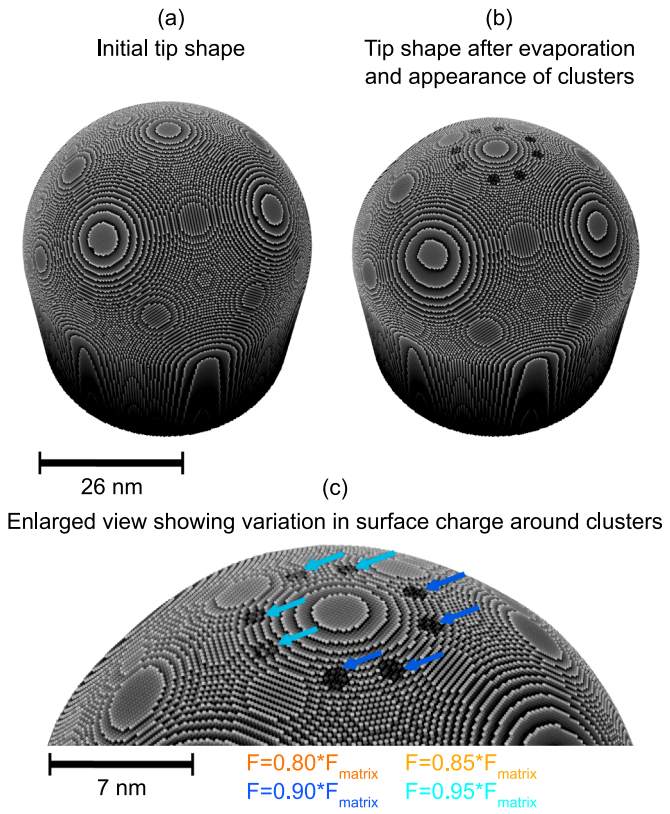

Fig. 2. (a) Initial tip shape and distribution of surface charge for APT evaporation trajectory simulations. (b) Tip shape and surface charge after evaporation and appearance of first layer of clusters with radius of 1 nm and (c) enlarged view of surface charge distribution in vicinity of clusters. N.B. the 0.80 x F_{Matrix} and 0.85 x F_{Matrix} clusters are located in equivalent positions but 5.3 nm below the 0.90 x F_{Matrix} and 0.95 x F_{Matrix} clusters and so are not visible in this image.

reconstructed using GPM_3DSAT Software and standard algorithms [63]. A detection efficiency of 0.52 was accounted for by random sampling of the data to remove 48 % of the atoms. Random perturbations in the x and y co-ordinates of the atoms were then applied for reasons stated in Section 4.4 APT Simulations. The perturbations were applied as described in Section 3.1 Simulations of Limited Spatial Precision in APT, for σ values of 0.4 nm and 0.6 nm.

Cluster searches were conducted using the Maximum Separation and Iso-Position methods. The same procedures described in Section 2.2.1 Analysis of Clusters in Neutron-Irradiated Steels were followed, with the search parameters shown in Table 4. The Fe content of the clusters measured by each technique was then calculated.

4. Results

4.1. Literature search

The data extracted from the literature showed that the range of reported Fe contents of clusters formed in RPVs under neutron irradiation is between 0 at.% and 92 at.%. As discussed in the introduction, the articles that report Fe contents of 0 at.% often do so despite their raw measured value of Fe being greater than 0 at.%. When only the raw measured Fe contents are considered, the range of Fe contents is reduced to between 38 at.% and 92 at.%. As previous round robin studies on model data have shown that the application of different cluster search algorithms or the application of same algorithm by different users can lead to large variations in quantitative results [47,64], this may explain some or all of the variation in the measured Fe contents reported in the literature.

Of the 145 individual datapoints that reported the raw measured Fe composition of the clusters, 63 used the maximum separation cluster search method, 39 used the Recursive Search method, 16 used Iso-Position method, 15 used the Composition Method, and 12 did not report which cluster search method was used. The distribution of measured Fe contents for each of these cluster search methods is presented in Fig. 3. It is apparent that datapoints that use the maximum separation search method appear to have the broadest range of measured Fe contents, but that their mean measured Fe content is below the mean for both the Iso-Position and Composition Method. Meanwhile, the Recursive Search algorithm, which was employed in two separate studies by the same group of researchers led to a very narrow range of measured Fe contents (54.7 at.% to 61.8 at.%.).

Whilst it appears from Fig. 3 that cluster search method may impact the measured levels of Fe within solute clusters in RPV steels, it is critical that we consider other potential explanatory variables. For example, one can imagine that alloys irradiated to low dose may have less developed solute clusters, which contain more Fe. Alternatively, alloys with high nominal solute levels may exceed the solubility limit of Mn + Ni + Si in Fe and therefore precipitate phases that contain little-to-no Fe in them.

Multiple linear regression is a statistical technique that permits determination of the influence of multiple explanatory variables,

Table 4
Parameters used for cluster searches in the simulated datasets using the Maximum Separation and Iso-Position methods.

σ (nm)	Original Cluster Fe Content (at. %)	Search Method	Core Ions	Dmax (nm)	Order (ions)	Nmin	L (nm)	E (nm)	Concentration Threshold (at.%)	Atomic Distance (nm)	Nmin	D_{Ero1} (nm)	D_{Ero2} (nm)
0.4	0	Maximum	Ni,	0.50	1	20	0.40	0.40					
	25	Separation	Mn, Si	0.50	1	20	0.40	0.40					
	50			0.55	1	20	0.45	0.45					
	75			0.70	1	20	0.70	0.65					
	0	Iso-Position	Ni,						4–6	0.40	10	0.69–0.90	0.93–1.26
	25		Mn, Si						4–6	0.40	10	0.66–0.93	0.99–1.11
	50								4–6	0.40	10	0.69–0.84	0.96–1.08
	75								2–6	0.40	10	0.42–0.69	0.78–1.02
0.6	0	Maximum	Ni,	0.50	1	20	0.40	0.40					
	25	Separation	Mn, Si	0.50	1	20	0.40	0.40					
	50			0.55	1	20	0.45	0.45					
	75			0.70	1	20	0.70	0.65					
	0	Iso-Position	Ni,						6–8	0.40	10	0.42–0.60	0.84–0.93
	25		Mn, Si						6–8	0.40	10	0.45–0.54	0.69–0.81
	50								6–8	0.40	10	0.42–0.60	0.57–0.87
	75								2–6	0.40	10	0.33–0.57	0.69–1.08

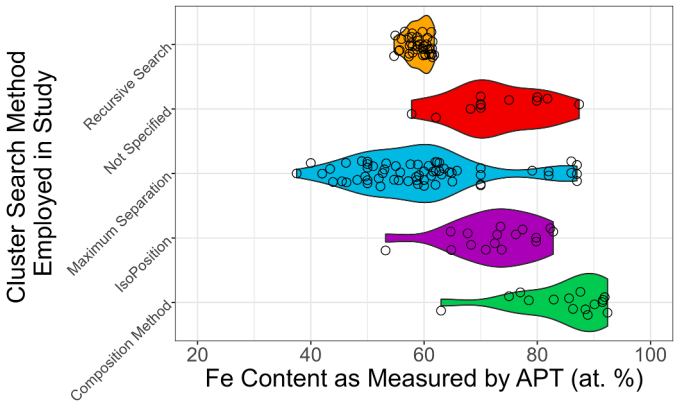

Fig. 3. Combined scatter and violin plots showing the distribution of the Fe contents of solute clusters, as measured by APT and reported within the literature, for the various cluster search algorithms employed.

including both numeric and categorical types, on a response variable. Application to solute clusters in RPV steels could enable the role of: nominal Fe, Mn, Ni, Si, and Cu contents; neutron irradiation fluence, flux, and temperature; APT instrument used; the cluster search method employed; and measured cluster radius on the measured cluster contents of Fe to be investigated. We attempted to perform this analysis on the data generated from the systematic review of the literature. However, in order to perform this statistical analysis in a robust fashion, certain criteria must be met. These include that the data are normally distributed and that independent variables are not co-dependent with one another.

Fig. 4 shows that, whilst there appears to be a trend of decreasing measured Fe content with increasing nominal solute alloy content, there is co-dependency between the nominal solute content of alloys and the cluster search method applied to them, with the maximum separation method applied much more frequently than other search algorithms to

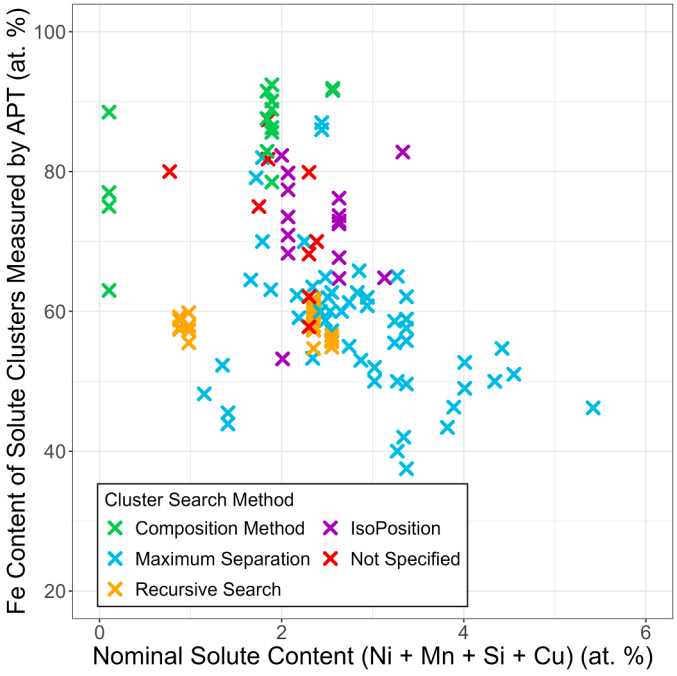

Fig. 4. Relationship between nominal solute content of Ni + Mn + Si + Cu and the Fe content of solute clusters measured by APT. The colour of each datapoint represents the cluster search method used to identify the solute clusters for each measurement. The co-dependency of bulk solute content and cluster search method can be seen.

alloys containing high solute levels. This co-dependency means it is not possible to determine whether the measured Fe content is changing as a result of varying nominal solute content or the application of different cluster search algorithms. Another issue is that inclusion of other potential explanatory variables, such as measured cluster radius, is complicated by the fact that the reported values for these variables are often not directly comparable since they are obtained using different methods by different researchers (e.g. equivalent radius vs Guinier radius). Combined with the observation that independent variables such as fluence and flux were not normally distributed, it was concluded that performing regression analyses on the data would be erroneous and unlikely to lead to reliable outcomes.

4.2. APT experiments

4.2.1. Lateral precision measurements

To determine how significant a role the application of different cluster search algorithms has on the measured Fe content of solute clusters in APT data, the Maximum Separation and Iso-Position algorithms were both applied to experimental data of two alloys that contained different nominal levels of solute.

The lateral precision was determined on a range of LEAP instruments that are commonly used to characterise RPV steels. The measured precisions are shown in Table 5 and are consistent with previous observations, which estimate an effective precision in APT experiments of between 0.5 nm and 1.25 nm [46]. There is a trend for improved spatial precision at lower operating temperatures and in voltage-pulsing mode when compared to laser-pulsing mode [65]. It is also confirmed that straight flight path instruments have significantly better spatial precision than reflectron-fitted instruments [66]. It is important to stress that these measurements of spatial precision were conducted in the vicinity of crystallographic poles, where it is known the APT data has its highest precision [67]. The average lateral precision within each dataset is expected to be worse than these values, especially as the distance from crystallographic poles increases. The precision will also be negatively impacted in regions affected by trajectory aberrations (e.g. around solute clusters that evaporate non-uniformly compared to the matrix), since these regions are subjected to lateral precision degradation from multiple phenomena.

4.2.2. Cluster search results

Fig. 5 shows the APT results for Alloy HN and Alloy LN. The nature of

Table 5
Measured lateral precisions in datasets of ferritic steels acquired using a variety of LEAP instruments under a range of analysis conditions. N.B. Since lateral precision is likely to depend on the material undergoing analysis [68] and will likely vary with distance from crystallographic poles, readers should exercise great caution about inferring the lateral precision of their experiments from the values presented here.

Instrument	Alloy	Operating Mode	Temperature (K)	Lateral Precision σ (nm)
LEAP 5000 XS	Fe-1at% Cu	Laser	50	1.10
	Fe-1at% Cu	Voltage	50	0.18
	RPV steel	Voltage	50	0.21
LEAP 5000 XR	RPV steel	Voltage	50	0.38
	RPV Steel	Voltage	60	0.34
	Fe-1at% Cu	Voltage	50	0.35
LEAP 4000X HR	RPV steel	Voltage	60	0.40–0.85
	RPV steel	Voltage	55	0.45

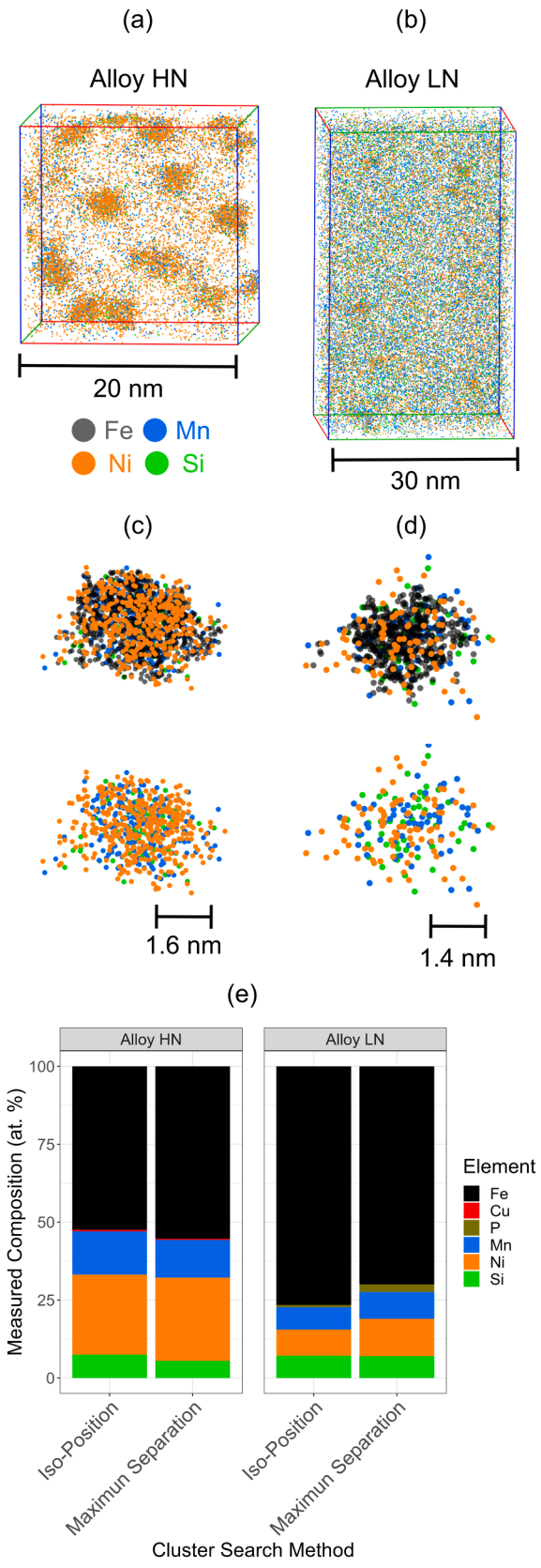

Fig. 5. Sub-volumes of APT datasets showing Ni-Mn-Sn clustering in (a) Alloy HN and (b) Alloy LN. Enlarged view of individual clusters in (c) Alloy HN (d) Alloy LN, with and without Fe displayed. (e) Shows the average composition of clusters in Alloy HN and Alloy LN, as measured using the Iso-Position and Maximum Separation cluster search algorithms. N.B. no Fe atoms are displayed in (a) and (b) for clarity.

the clustering is visibly different; it is shown in the dataset sub-volumes in Fig. 5(a) and (b) that there is much stronger contrast between the clusters and the matrix in Alloy HN than in Alloy LN. Fig. 5(c) and (d) show an enlarged view of an individual cluster from each dataset, both with and without Fe atoms displayed. The clusters in Alloy HN appear to be much denser in nature than the clusters in Alloy LN, whilst there also appears to be a larger fraction of Fe in the Alloy LN clusters.

Cluster searches were performed using the Iso-Position and Maximum Separation methods and the mean equivalent cluster radius was calculated in each alloy (Table 6). This size was compared to the size of the clusters measured along the z-axis in the reconstruction, where APT is known to have its best spatial precision provided the reconstruction is accurate [69]. The calculated sizes were reasonably similar between the two cluster search methods, although there were slightly larger differences between them when applied to data from Alloy LN. The choice as to whether to include or exclude Fe can have a large impact on the average cluster size that is calculated, particularly in the case of small clusters or clusters that contain large fractions of detected Fe. It is noteworthy that the measured cluster size along the z-axis in the reconstruction was most closely correlated to the equivalent radius when excluding Fe for Alloy HN, whilst the cluster sizes in Alloy LN correlated with calculations that include some Fe.

Compositional measurements, performed after cluster searches were conducted using the Iso-Position and Maximum Separation methods, are presented in Fig. 5(e). The compositional measurements are consistent between the two methods. More Fe was measured, by both methods, in the clusters in Alloy LN than in Alloy HN. The fact that Maximum Separation measures more P in the clusters in Alloy LN is likely due to the inclusion of a detected cluster that was considered as edge in the Iso-Position dataset.

4.3. Simulations of limited spatial precision in APT

Fig. 6 shows how the measured Fe content of clusters varies as a function of cluster radius and lateral precision for clusters that originally contained 0 at.% Fe. These data show that more spurious Fe is measured in the case of small clusters and at worse lateral precisions. The ratio between cluster size and lateral precision is therefore likely to have an impact on the erroneous levels of matrix Fe that is introduced into the solute clusters.

Fig. 7 shows how the measured Fe content varies as a function of the ratio between cluster radius and lateral precision, and also as a function of the original Fe content of the clusters. Limited lateral precision can introduce significant amounts of Fe into the original cluster volumes. There are some differences in the measured Fe content of the clusters depending on whether the entire original cluster volume is considered or

Table 6
Measured cluster sizes for Alloy HN and Alloy LN, calculated including and excluding Fe using both Iso-Position and Maximum Separation cluster search methods, and by measuring the cluster size in the z-axis of the reconstructed data. The measured atomic density within the clusters vs the matrix is also provided.

Alloy	Fe Included in Calculation	Average Equivalent Radius (nm)		Average Radius Measured in Reconstruction z-axis (nm)	Ratio of Atomic Density of Clusters vs Matrix
		Iso-Position	Maximum Separation		
HN	Yes	1.9 ± 0.3	2.1 ± 0.2	1.4 ± 0.1	2
	No	1.5 ± 0.3	1.6 ± 0.2		
LN	Yes	1.3 ± 0.3	1.6 ± 0.1	1.1 ± 0.2	1.5
	No	0.8 ± 0.2	1.1 ± 0.1		

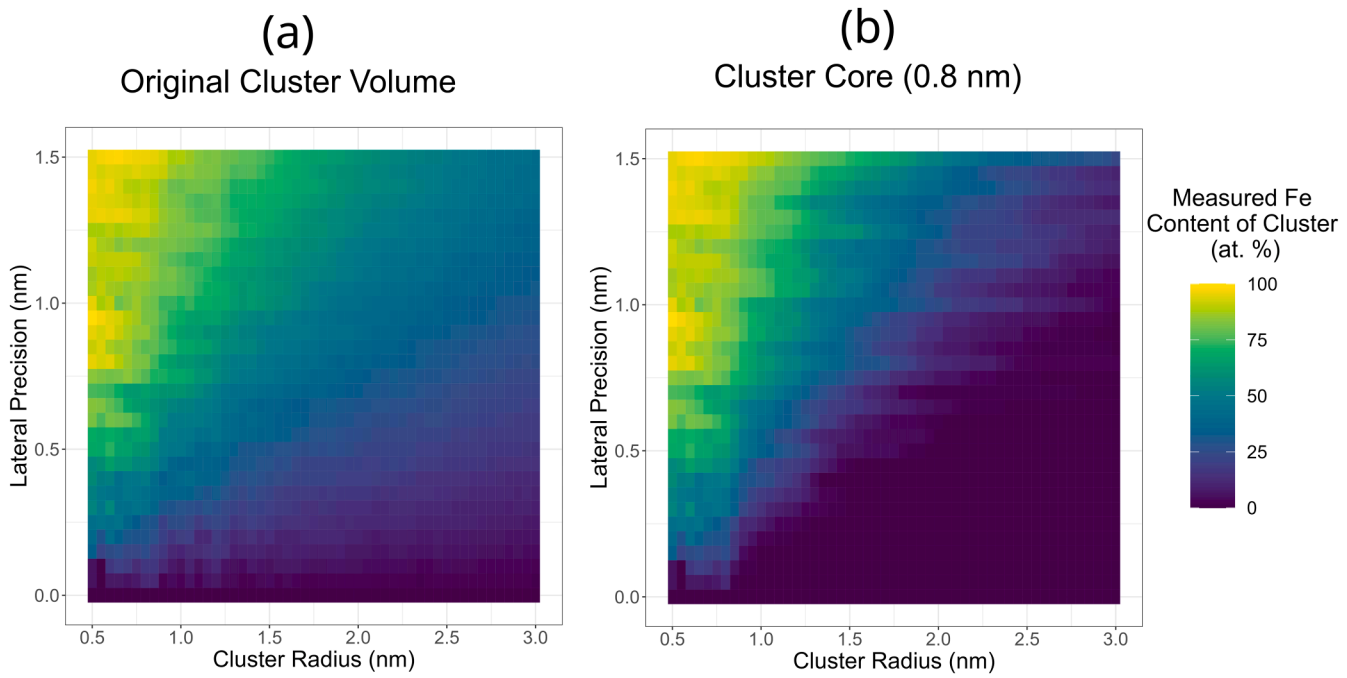

Fig. 6. Heatmap depicting the variation in measured Fe content of clusters that originally contain 0 at.% Fe as a function of cluster radius and lateral precision. (a) Shows the composition within the original cluster volume (b) shows the composition within the cluster core.

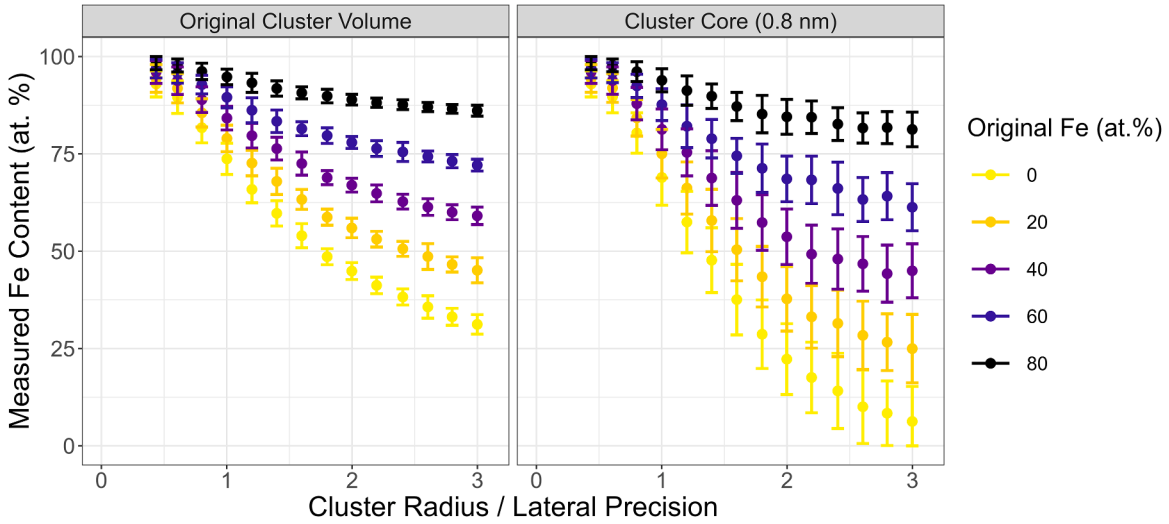

Fig. 7. Scatter plots showing the variation in measured Fe content (at.%) of clusters as a function of the Cluster Radius/Lateral Precision ratio. For clarity and to assist the reader, the data has been binned such that each data point represents the mean value of all datapoints within a bin width of 0.2 on the x-axis (i.e. the Cluster Radius/Lateral Precision value at 1 is the mean value for all datapoints with a Cluster Radius / Lateral Precision between 0.9 and 1.1). Error bars represent the standard deviation in the measured values of Fe within each bin.

just the cluster core. Firstly, the cluster core measurements have higher variance, which likely arises since fewer atoms are used for the compositional calculations, and so these measurements are more susceptible to small changes in the number of Fe or cluster atoms. Secondly, the core composition method appears to accurately determine the composition of the features once the clusters are more than three times the size of lateral precision. This is not the case for the measurements made by considering the original cluster volume, which consistently overestimates the Fe content of the cluster when compared to the true Fe levels. Whilst these simulations show that the amount of spurious Fe introduced into solute clusters is dependent upon both the cluster radius and lateral precision of the experiment, readers should be aware that direct comparison to experimental data requires careful consideration. One reason for this is that these simulations assume the clusters are not affected by trajectory aberrations, which would artificially reduce their effective radius. Secondly, lateral precision in APT datasets is most often measured at crystallographic poles and the precision in the vicinity of solute clusters is often unknown.

4.4. APT simulations

Examples of the clusters that had an initial radius of 1 nm and underwent simulated field evaporation are shown in Fig. 8. It can be seen that all cluster types appear compressed in the x-y direction, despite being spherical at the beginning of the simulation. The degree of compression in x-y increases as the ratio of $F_{Cluster}/F_{Matrix}$ of the atoms

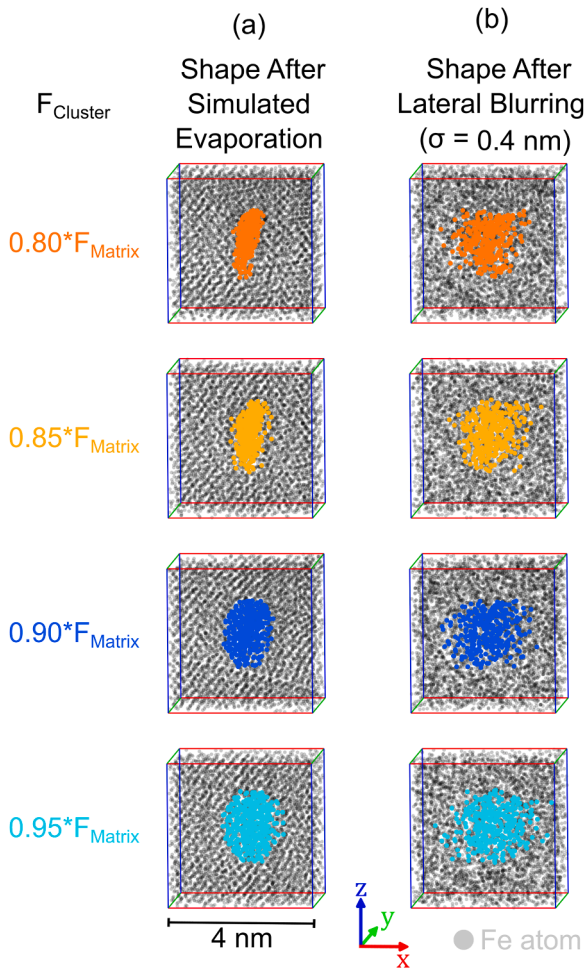

Fig. 8. How the reconstructed shape of initially spherical clusters (radius = 1 nm) varies as a function of the ratio between the evaporation field of the clusters ($F_{Cluster}$) and the evaporation field of the matrix (F_{Matrix}) (a) before and (b) after lateral blurring is applied.

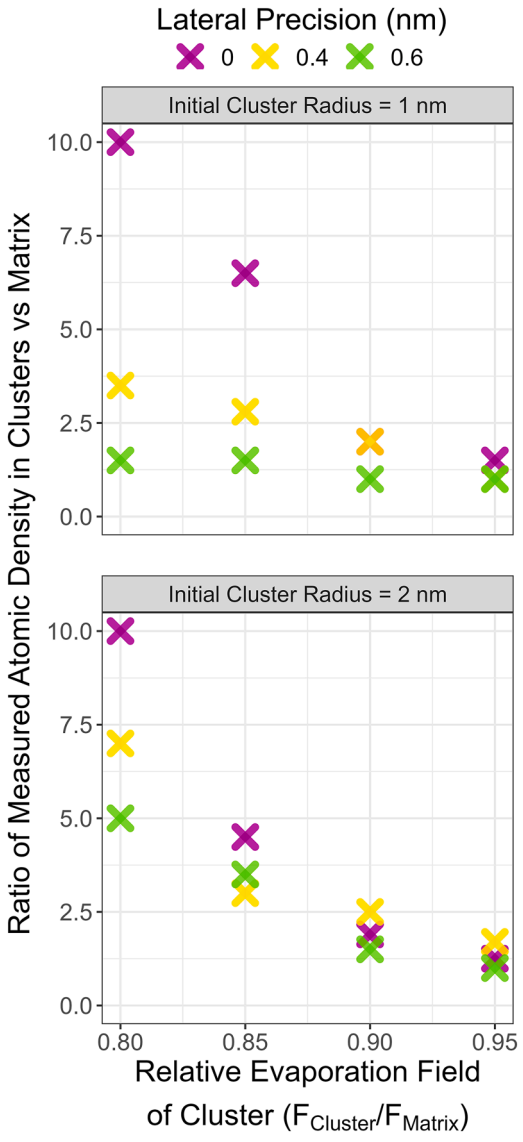

Fig. 9. Graphs showing the ratio between the atomic density measured within clusters compared to the matrix in clusters that underwent simulated field evaporation. Change in measured atomic density is shown to vary with initial cluster radius, relative evaporation field of the clusters, and lateral precision.

within the clusters decreases. This compression is not observed in experimental data for Mn-Ni-Si-rich features in RPV steels (Fig. 5) but this is likely to be because the simulation used in this study does not account for all of the aforementioned processes that negatively impact lateral precision such as atomic roll-up. Further evidence that our simulations are failing to capture all of the phenomena that impact the accuracy of spatial positioning is that the measured spatial precision in the simulations is much better than that which is experimentally-observed in pure materials. Once we estimate these effects by applying Gaussian noise perturbations in the x and y co-ordinates of the atoms, Fig. 8(b) shows that the shapes of the simulated clusters very closely resemble those observed experimentally. In addition, Fig. 9 demonstrates that the clusters that have undergone simulated field evaporation and reconstruction still display higher atomic densities than the surrounding matrix, which is something that is often observed experimentally [24]. The ratio of cluster:matrix density is shown to decrease as a function of worsening lateral precision and also as $F_{Cluster}$ and F_{Matrix} become more similar to one another, for the range of evaporation field differences explored in this study.

Whilst the application of Gaussian noise perturbations in the x and y co-ordinates of the atoms does not directly represent what is physically happening during field evaporation and the subsequent flight path of ions, the authors believe that this assumption is a reasonable approximation of the effect that other phenomena have on the recorded spatial position of atoms in experimental data. The model that we implemented here could be extended in the future to incorporate slight thermal velocities or roll-up of atoms prior to their evaporation from the surface, but this is beyond the scope of this study.

Compositional measurements of the clusters revealed that both cluster search methods incorrectly characterise the solute clusters, with more Fe being measured in the clusters than was present in the clusters prior to field evaporation, except for the case when the Iso-Position method is used to determine the composition of large clusters ($r = 2$ nm) that have a similar $F_{Cluster}$ to the matrix. The degree of this over-measurement is visible in Fig. 10 and gets worse with smaller clusters, larger values of σ, and with greater differences between $F_{Cluster}$ and F_{Matrix}.

The Maximum Separation and Iso-Position methods are reasonably consistent with one another for the 1 nm radius clusters, but there is a large divergence in the measured composition for the 2 nm radius clusters. This difference between the Maximum Separation and Iso-Position methods for the $r = 2$ nm clusters is due to the fact that there remains a core region of these clusters that does not contain matrix atoms (Fig. 11). The Iso-Position method applies two erosion steps for its

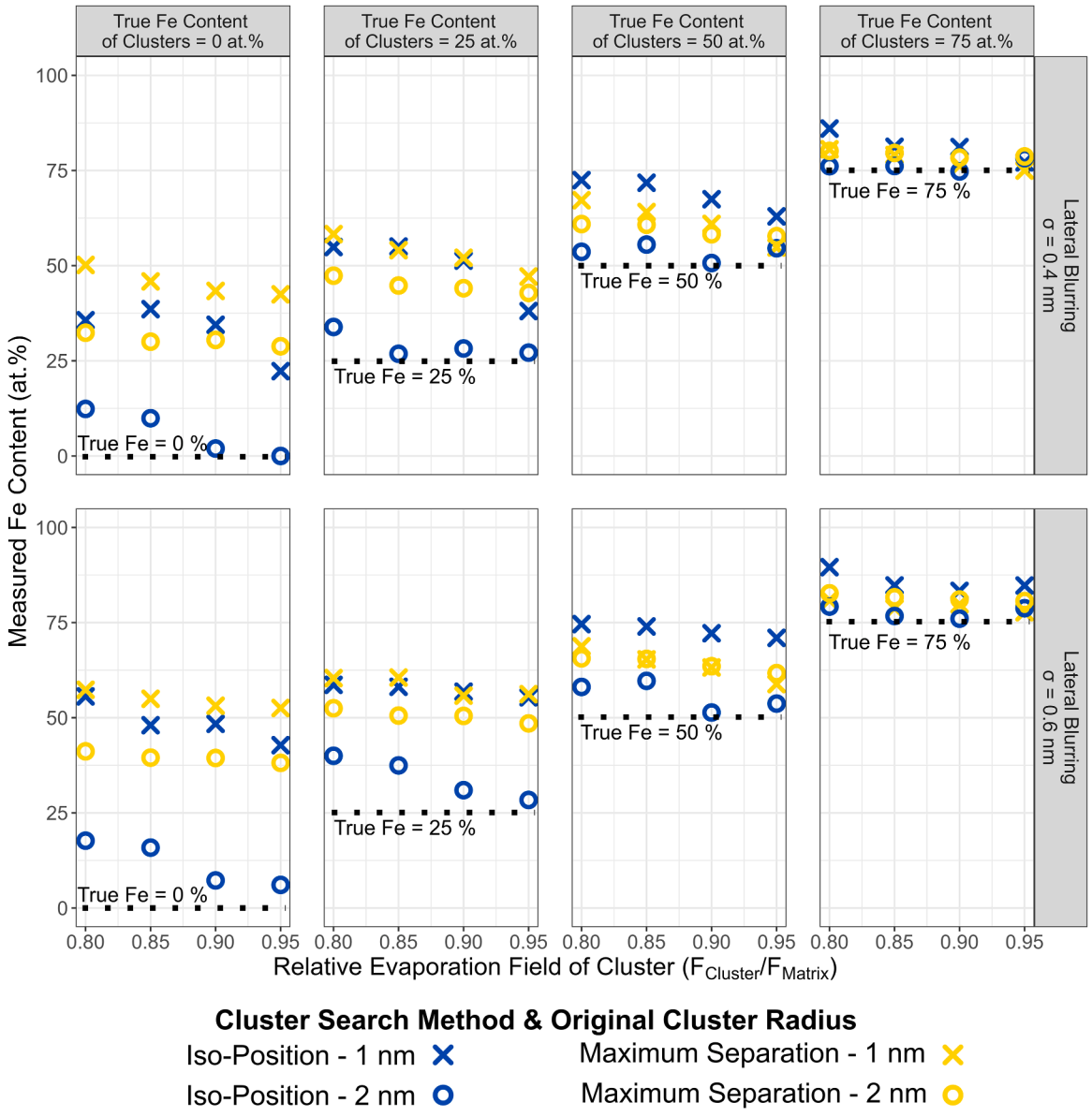

Fig. 10. How the measured composition of Fe varies in clusters that undergo simulated evaporation as a function of: true Fe content; the relative evaporation field of the cluster vs the matrix; degree of lateral blurring; original cluster radius; and cluster search method employed.

compositional calculations and it is able to identify this core region of the $r = 2$ nm clusters, which is free from aberrant matrix atoms. Meanwhile, the Maximum Separation method only applies one erosion step for its compositional calculations and so the edge of the clusters, which are subjected to significant distortion, are included in the cluster search results and the compositional calculations.

Fig. 11 demonstrates that the limited accuracy of the spatial positioning of atoms in APT is likely responsible for the introduction of the majority of the aberrant matrix atoms that are observed in clusters that have a lower evaporation field than the matrix. The extent of this effect will increase with decreasing cluster size and increasing values of σ, and clusters with an initial radius of less than 2 nm are highly likely to have aberrant matrix atoms present in their cores.

5. Discussion

The cause of the large variance in the APT-measured Fe contents of clusters that form under neutron irradiation in RPV steels has been a contentious subject for several years. The approach taken here was to combine a systematic review of the literature with experimental data, different data analysis procedures, and computational simulations to investigate what is responsible for this variance. Combining these approaches and using the results from each of them to inform and guide interpretation of the data permits a more robust assessment of what the true Fe contents of these features are likely to be.

The measured Fe contents in the literature were shown to be correlated with both the nominal Mn + Ni + Si + Cu levels but also the cluster search method employed to analyse the data, since the cluster search method and nominal Mn + Ni + Si + Cu levels were co-dependent with one another. The combination of a limited number of studies and the large number of variables that change between them complicates the application of quantitative statistical analyses. This demonstrates the utility of studies that are designed to systematically investigate the effects of changes in specific variables, although this is not always possible due to the fact that RPV samples that are available to study often originate from different base alloys and also from surveillance capsules in reactors that operate under dissimilar conditions.

Previous round-robin tests in the APT community have shown that

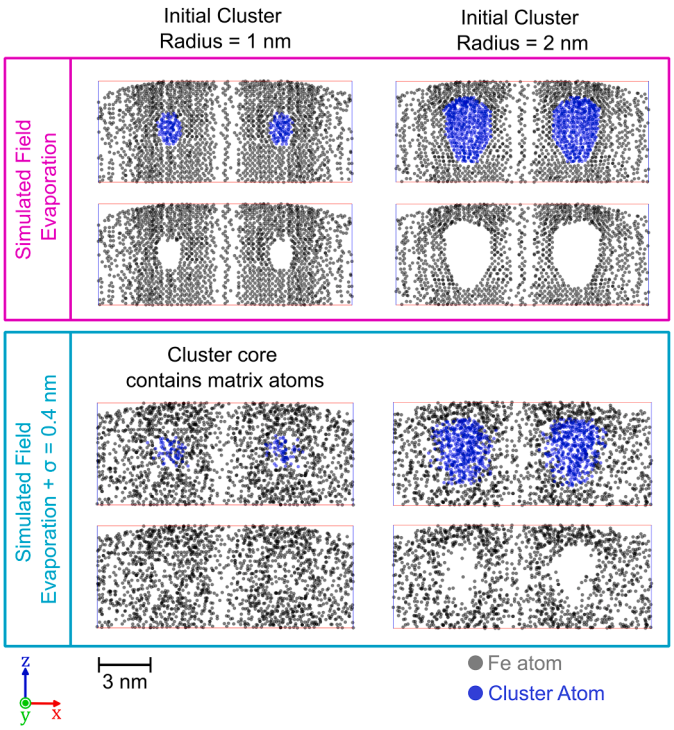

Fig. 11. Atom maps showing 0.3 nm thick slices through initially spherical clusters that have undergone simulated field evaporation ($F_{Cluster}$ = 0.90 x F_{Matrix}). The cluster core is free of matrix atoms after simulated field evaporation but, after accounting for the imperfect spatial positioning, large numbers of matrix atoms are mixed within the clusters that have an initial radius of 1 nm.

different data analysts or the application of different search algorithms can significantly impact measurements of solute clusters [38,47]. Our results show that it is unlikely that application of different cluster search algorithms fully explains the differences in published measured Fe contents, especially in the case of small clusters typically observed in RPV steels. Our results show reasonable consistency between the Maximum Separation and Iso-Position methods in both experimentally-acquired data (Fig. 5) and for small clusters (r = 1 nm) that have undergone simulated field evaporation (Fig. 10). It should be noted that whilst the Maximum Separation and Iso-Position methods were applied independently, they were applied by researchers with significant experience of using APT to characterise solute clusters in RPV steels; this may explain why the results were more consistent than may have been expected based upon round-robin studies where operators may not have similar levels of experience with the studied system.

Despite the consistency between the compositional measurements made by the two cluster search methods, the imperfect spatial positioning of atoms in the reconstructed data [26,53,54] appears to be responsible for erroneously leading to over-measurement of the solute clusters' true Fe content. The simulations that represent the effect of limited spatial precision in APT demonstrate that the imperfect lateral positioning of atoms can introduce very large amounts of spurious Fe into Mn-Ni-Si-rich features, and that this problem is strongly dependent on the ratio of cluster radius ($r_{Cluster}$) to lateral precision (σ) (Fig. 6& Fig. 7).

This highlights the critical importance of APT operators being aware of the fundamental limitations of the technique and resulting uncertainties that are inherent when analysing small solute clusters [46,64]. The negative influence of limited lateral precision demonstrates the necessity to optimise spatial positioning through careful selection of experimental parameters, and also the importance of accurately calibrating one's APT reconstructions. Estimating and reporting the lateral precision of APT datasets alongside measured Fe content is currently very uncommon, but this would help in the assessment as to how much Fe measured within the clusters is likely incorporated due to limited spatial positioning accuracy in APT experiments.

The accuracy of the spatial positioning of atoms in the reconstructed data can also be negatively impacted by trajectory aberrations, which arise due to differences in the evaporation fields of different volumes of a material. Our estimations of $F_{Cluster}$ from charge-state-ratio measurements, and the fact that clusters in RPV steels often demonstrate higher atomic density than the surrounding matrix in APT reconstructions [24], indicate that Mn-Ni-Si-rich features are likely to be lower field than the surrounding matrix. The simulations in Fig. 8 show that the large deformations in reconstructed cluster shape due to differences in $F_{Cluster}$ and F_{Matrix} can be obscured by the limited accuracy of spatial positioning in APT.

It should be noted that it has been previously shown that the impact of trajectory aberrations on cluster shape and compositional bias is dependent on the ratio between $r_{Cluster}$ / r_{Tip} and $F_{Cluster}$ / F_{Matrix} [56,61], and that this effect becomes more pronounced as the ratio of $r_{Cluster}$ / r_{Tip} decreases or $F_{Cluster}$ / F_{Matrix} deviates from unity. Since the tip radii used in the simulations in this study likely represent the lower end of the size of RPV samples that are experimentally measured using APT, the degree of distortion for clusters of a given radius in experimental data may be larger than shown in Fig. 11 and that this may result in more aberrant matrix atoms being introduced into the features. One interesting observation in the simulated field evaporation datasets is that, despite significant distortion in the x-y plane, clusters dimensions in the z-direction remain fairly similar to their initial size. Therefore, measuring cluster size in the z-direction of APT datasets may provide a more reliable measure of size than calculating an equivalent radius for the clusters, assuming that the APT reconstruction itself is accurate and has been calibrated correctly.

Our results indicate that, whilst trajectory aberrations alone may sometimes introduce Fe into the solute clusters in reconstructed APT datasets, it is the limited accuracy of spatial positioning in APT due to other effects that is most responsible for the introduction of matrix atoms into clusters. We have shown that there is an exponential relationship between measured Fe content of clusters and the ratio of $r_{Cluster}/\sigma$; this is important to recognise for the small cluster radii typically observed in RPV steels and with the lateral spatial precisions typically recorded on reflectron-fitted LEAP instruments. However, it is also noteworthy that the compression of clusters in the x-y plane due to local magnification (Fig. 8) reduces the effective radius of clusters in the plane in which APT spatial precision is least accurate, and this is likely to make compositional measurements of the solute clusters more susceptible to the deleterious effects of the limited spatial positioning in APT.

Fig. 10 shows that the combination of trajectory aberrations and limited spatial positioning accuracy due to other effects leads to the incorrect compositional measurement of solute clusters, with the measured Fe content higher than the true Fe content in nearly every simulated case. This overestimation is very pronounced at smaller cluster sizes. Combining these results with experimental observations, and estimations of spatial positioning in the vicinity of poles (Table 5), enables us to estimate what the true Fe content of the solute clusters in RPV steels may be.

Maximum Separation and Iso-Position cluster search methods both measure more Fe in the clusters in Alloy LN (~75 at.%) than in Alloy HN (~50 at.%) (Fig. 5). The results of the simulations presented in Fig. 10 indicate that the clusters in both alloys are in the size range that will be affected by the imperfect spatial precision of APT experiments and that the experimentally-measured Fe contents are overestimations of the true Fe contents of these solute clusters. Combining our experimental results with the simulations conducted in this study enable us to estimate the extent of Fe overmeasurement from APT and therefore we are able to approximate the true Fe content of the solute clusters in these alloys.

For Alloy HN, the clusters have an average atomic density that is twice that of the matrix and an average radius of 1.4 nm, when measured

in the z-direction (Table 6). Accounting for the estimated lateral precision, Fig. 9 indicates that clusters of this size and atomic density likely have a relative evaporation field of approximately 0.85 compared to the matrix. The experimentally-measured cluster compositions (Fig. 5) correspond to the simulations for clusters that originally contain between 0 and 25 at.% Fe (Fig. 10). Meanwhile, the clusters in Alloy LN have an average size of 1.1 nm and an atomic density that is 1.5 times that of the matrix. Fig. 9 suggests that these features likely have a $F_{Cluster} = 0.80$ to 0.85 x F_{Matrix}. The simulations that most closely match the experimentally-measured Fe content of these clusters are simulations of clusters that originally contain 50 at.% Fe (Fig. 10).

Whilst the above process enables us to estimate the Fe content of the clusters, uncertainties remain as to the spatial precision in the vicinity of clusters and the true cluster size in the experimental datasets. Since spatial precision can have a strong influence on measured Fe content, it is challenging to precisely state a value for the Fe content of the clusters with confidence. However, it can be stated that the data presented in this work suggests that the clusters in Alloy HN contain between 0 and 25 at.% Fe whilst the clusters in Alloy LN contain around 50 at.% Fe. These estimates are further supported by the direct measurements of cluster size in the z-direction in the datasets for both alloys; these measurements indicate that the calculated equivalent radius including Fe predicts a much larger size than is observed in Alloy HN but that radii of clusters in Alloy LN are between those calculated when including and excluding all Fe atoms (Table 6). This comparison of equivalent radii and measured radii in the z-direction indicates that the majority of the Fe in the clusters in Alloy HN may be the result of aberrations whilst some of the Fe atoms detected within the clusters in Alloy LN may be truly present in the clusters, which is consistent with the results from the previous paragraphs.

Because uncertainties remain around precisely how accurate lateral positioning of atoms is in the vicinity of these features in experimentally-acquired data, it would not be reasonable to provide a more precise value for the estimated true Fe content of the features in each alloy. Whilst this is somewhat unsatisfactory, and leaves us with a range of ~0–50 at.% Fe for solute clusters that form under neutron irradiation in RPV steels, this is a large reduction on the range reported in the literature (0–92 at.%) and an improvement. However, we have demonstrated that multiple phenomena combine to reduce the accuracy of compositional measurements of solute clusters in RPV steels and that each of these must be considered when determining how representative measured cluster compositions are of the true cluster compositions. Therefore, it is critical that authors justify the assumptions they make when evaluating the true Fe content of the features they observe; these assumptions include providing measurements of tip radius alongside estimates of experimental lateral precision and the estimated evaporation field of the features compared to the matrix.

The difference in measured Fe content of clusters in Alloy LN and Alloy HN likely reflects a difference in the nature of clusters. Indeed, the clusters themselves are visibly different in each alloy. Fig. 5(c) and (d) show that the clusters in Alloy LN are much more diffuse and less densely clustered than those observed in Alloy HN. The source of this difference may be due to the differences in the nominal compositions of the two alloys, with Alloy HN containing much more bulk Mn, Ni, Si, and Cu (5.78 at.%) than Alloy LN (2.97 at.%). The solid solubility limit in α-Fe may be exceeded in the higher solute alloy and, as a result, lead to a transition from a radiation-induced formation mechanism in Alloy LN to a radiation-enhanced mechanism in Alloy HN. The potential of radiation-enhanced cluster formation is something that is not currently incorporated in some models that predict embrittlement of RPV steels during service [36], and may lead to the underprediction of mechanical property changes at extended operating times if steels are highly enriched in solutes. Another potential explanation for the differences in the nature of the clusters observed in the two alloys may be the different fluxes experienced during irradiation, with Alloy LN experiencing a higher neutron flux than Alloy HN. This increased dose rate for Alloy LN may be expected to lead to more radiation induced segregation [70], which is a possible alternative explanation for the higher Fe content of the clusters in Alloy LN compared to those observed in Alloy HN.

The wide range in measured Fe contents of solute clusters in the literature likely reflects a range in the true Fe contents of the features. Therefore, although this range is smaller in reality than has been previously reported, determining what the true range of Fe contents is in all literature samples is currently not possible due to the absence of certain information that is critical for making an informed assessment. If researchers were to report their measured Fe levels alongside other important parameters it would be possible to determine more precisely what the true range of Fe contents is in clusters in RPV steels; these parameters include: the estimated spatial precision of each dataset, tip radius, cluster identification method used, cluster size measured in z-direction of reconstruction, and atomic density of clusters compared to the matrix in reconstructed datasets. There is also a need for the evaporation field of phases predicted to be present in RPV steels, such as those from Refs. [34,62], to be determined for varying levels of Fe content and different stoichiometries. In irradiated alloys, the inclusion of interstitial atoms or vacancies will also impact the atomic density and the evaporation field of the features; a future study that incorporated these defects into field evaporation simulations would be useful in determining to what extent their presence further degrades lateral precision. The availability and implementation of an open-source cluster search algorithm with limited user input requirements that provides reproducible and repeatable measurements and is used by all researchers would also be beneficial. Whilst calls for this have long been made in the APT community [64], and some progress has been made [71], there is still no universally accepted approach that is available to be used by all researchers. This affects APT's ability to provide consistent results and is something that should be addressed as a matter of urgency.

6. Conclusions

The application of different data analysis protocols to experimental and simulated data show that the Fe content of solute clusters in RPV steels is almost certainly overestimated when measured by APT, especially in the case of clusters with radii smaller than 1.5 nm. This spurious Fe can be substantial in quantity, and is added to clusters due to the limited accuracy of the spatial positioning of APT.

In order to make accurate estimations of the true Fe content of the solute clusters in RPV steels, authors should ensure that they account for the phenomena discussed in this article. APT operators should be careful when interpreting analyses of small solute clusters and, if they wish to assess the accuracy of their Fe content measurements, should report experimental parameters that can significantly impact their compositional measurements. These parameters include but are not limited to: spatial precision of their reconstructed datasets, tip radius, evaporation field of clusters, and measured Fe content of clusters.

Another conclusion of this study is that not all of the variation in the literature values of Fe content in clusters observed in RPV steels can be explained by APT artefacts. Clusters in two RPV steels with non-identical nominal compositions and irradiated at different fluxes were shown to have different average measured levels of Fe. These differences may affect the formation mechanism of the features and, hence, the amount of Fe that is incorporated into the clusters. This has important implications, especially for models that predict cluster formation and growth, and mechanical property changes in RPV alloys at extended lifetimes.

CRediT authorship contribution statement

Benjamin M. Jenkins: Writing – review & editing, Writing – original draft, Visualization, Software, Methodology, Investigation, Funding acquisition, Formal analysis, Conceptualization. **Aidar Zakirov:** Writing – review & editing, Visualization, Methodology, Investigation, Formal

analysis, Conceptualization. **François Vurpillot:** Writing – review & editing, Visualization, Software, Methodology, Funding acquisition. **Auriane Etienne:** Writing – review & editing, Investigation, Formal analysis. **Cristelle Pareige:** Writing – review & editing, Funding acquisition. **Philippe Pareige:** Writing – review & editing, Funding acquisition. **Bertrand Radiguet:** Writing – review & editing, Methodology, Investigation, Funding acquisition, Formal analysis.

Declaration of competing interest

The authors declare that they have no known competing financial interests or personal relationships that could have appeared to influence the work reported in this paper.

Acknowledgements

This project has received funding from the European Union's Horizon 2020 research and innovation programme under the Marie Skłodowska-Curie grant agreement No. 101034329. Recipient of the WINNINGNormandy Program supported by the Normandy Region.

Experiments were performed on GENESIS platform instruments supported by the Région Haute-Normandie, the Métropole Rouen Normandie, the CNRS via LABEX EMC3 and the French National Research Agency as a part of the program "Investissements d'avenir" with the reference ANR-11-EQPX-0020.

This work was supported by the European Regional Fund (ERDF) and the Normandy Region through GENESIS+ and SATUP projects.

This work was partially supported by the CNRS Federation IRMA - FR 3095. This work was supported by the U.S. Department of Energy, Office of Nuclear Energy under DOE Idaho Operations Office Contract DE-AC07051D14517 as part of a Nuclear Science User Facilities experiment.

BMJ would like to express his thanks to Dr. Nick Riddle from Rolls Royce Plc. and Prof. Bob Odette from UCSB for providing the HN alloy used in this study and for fruitful discussions. AZ and BR thank R. Chaouadi, E. Stergar and I. Uytdenhouwen from SCK.CEN for providing the samples of LN alloy and for productive discussions.

Funding sources

This project has received funding from the European Union's Horizon 2020 research and innovation programme under the Marie Skłodowska-Curie grant agreement No. 101034329. Recipient of the WINNINGNormandy Program supported by the Normandy Region.

Experiments were performed on GENESIS platform instruments supported by the Région Haute-Normandie, the Métropole Rouen Normandie, the CNRS via LABEX EMC3 and the French National Research Agency as a part of the program "Investissements d'avenir" with the reference ANR-11-EQPX-0020. This work was supported by the European Regional Fund (ERDF) and the Normandy Region through GENESIS+ and SATUP projects. This work was partially supported by the CNRS Federation IRMA - FR 3095.

References

[1] R.M. Boothby, J.M. Hyde, H. Swan, D. Parfitt, K. Wilford, P. Lindner, SANS examination of irradiated RPV steel welds during in-situ annealing, J. Nucl. Mater. 461 (2015), https://doi.org/10.1016/j.jnucmat.2015.02.036.

[2] J.M. Hyde, M.G. Burke, G.D.W. Smith, P.D. Styman, H. Swan, K. Wilford, Uncertainties and assumptions associated with APT and SANS characterisation of irradiation damage in RPV steels, J. Nucl. Mater. 449 (2014) 308–314, https://doi.org/10.1016/j.jnucmat.2013.07.029.

[3] P.D. Edmondson, M.K. Miller, K.A. Powers, R.K. Nanstad, Atom probe tomography characterization of neutron irradiated surveillance samples from the R. E. Ginna reactor pressure vessel, J. Nucl. Mater. 470 (2016) 147–154, https://doi.org/10.1016/j.jnucmat.2015.12.038.

[4] P.D. Edmondson, C.M. Parish, R.K. Nanstad, Using complimentary microscopy methods to examine Ni-Mn-Si-precipitates in highly-irradiated reactor pressure vessel steels, Acta Mater. 134 (2017) 31–39, https://doi.org/10.1016/j.actamat.2017.05.043.

[5] K. Osamura, H. Okuda, M. Takashima, K. Asano, M. Furusaka, Small-angle neutron scattering study of phase decomoposition in Fe-Cu binary alloy, Mater. Trans. JIM 34 (1993) 305.

[6] K. Osamura, H. Okuda, K. Asano, M. Furusaka, K. Kishida, F. Kurosawa, R. Uemori, SANS study of phase decomposition in Fe-Cu Alloy with Ni and Mn addition, ISIJ Int. 34 (1994) 346–354.

[7] M.K. Miller, D. Hoelzer, F. Ebrahimi, J.R. Hawthorne, M.G. Burke, Characterization of irradiated model pressure vessel steels, Journal de Physique Colloques 48 (1987) 423.

[8] M.G. Burke, M. Watanabe, D.B. Williams, J.M. Hyde, Quantitative characterization of nanoprecipitates in irradiated low-alloy steels: advances in the application of FEG-STEM quantitative microanalysis to real materials, J. Mater. Sci. 41 (2006) 4512–4522, https://doi.org/10.1007/s10853-006-0084-x.

[9] F. Bergner, M. Lambrecht, A. Ulbricht, A. Almazouzi, Comparative small-angle neutron scattering study of neutron-irradiated Fe, Fe-based alloys and a pressure vessel steel, J. Nucl. Mater. 399 (2010) 129–136, https://doi.org/10.1016/j.jnucmat.2009.11.011.

[10] G.S. Was, M. Hash, R.G. Odette, Hardening and microstructure evolution in proton-irradiated model and commercial pressure-vessel steels, Philos. Mag. 85 (2005), https://doi.org/10.1080/14786430412331319974.

[11] P. Pareige, J.-C. Van Duysen, P. Auger, An APFIM study of the microstructure of a ferrite alloy after high fluence neutron irradiation, Appl. Surf. Sci. 67 (1993) 342–347, https://doi.org/10.1016/0169-4332(93)90336-A.

[12] M.K. Miller, M.G. Burke, An atom probe field ion microscopy study of neutron-irradiated pressure vessel steels, J. Nucl. Mater. 195 (1992) 68–82, https://doi.org/10.1016/0022-3115(92)90364-Q.

[13] M.K. Miller, P. Pareige, M.G. Burke, Understanding pressure vessel steels: an atom probe perspective, Mater. Charact. 44 (2000) 235–254, https://doi.org/10.1016/S1044-5803(99)00056-X.

[14] A. Morley, G. Sha, S. Hirosawa, A. Cerezo, G.D.W. Smith, Determining the composition of small features in atom probe: bcc Cu-rich precipitates in an Fe-rich matrix, Ultramicroscopy. 109 (2009) 535–540, https://doi.org/10.1016/j.ultramic.2008.09.010.

[15] P.D. Styman, J.M. Hyde, A. Morley, K. Wilford, N. Riddle, G.D.W. Smith, The effect of Ni on the microstructural evolution of high Cu reactor pressure vessel steel welds after thermal ageing for up to 100,000 h, Mater. Sci. Eng. A 736 (2018) 111–119, https://doi.org/10.1016/j.msea.2018.08.063.

[16] P. Pareige, R.E. Stoller, K.F. Russell, M.K. Miller, Atom probe characterization of the microstructure of nuclear pressure vessel surveillance materials after neutron irradiation and after annealing treatments, J. Nucl. Mater. 249 (1997) 165–174, https://doi.org/10.1016/S0022-3115(97)00215-8.

[17] T. Toyama, Y. Nagai, Z. Tang, M. Hasegawa, A. Almazouzi, E. van Walle, R. Gerard, Nanostructural evolution in surveillance test specimens of a commercial nuclear reactor pressure vessel studied by three-dimensional atom probe and positron annihilation, Acta Mater. 55 (2007), https://doi.org/10.1016/j.actamat.2007.08.047.

[18] N. Almirall, P. Wells, T. Yamamoto, K. Wilford, T. Williams, N. Riddle, G.R. Odette, Precipitation and hardening in irradiated low alloy steels with a wide range of Ni and Mn compositions, Acta Materialia Manuscript (2018) 119–128, https://doi.org/10.1016/j.actamat.2019.08.027.

[19] P.B. Wells, T. Yamamoto, B. Miller, T. Milot, J. Cole, Y. Wu, G.R. Odette, Evolution of manganese-nickel-silicon-dominated phases in highly irradiated reactor pressure vessel steels, Acta Mater. 80 (2014) 205–219, https://doi.org/10.1016/j.actamat.2014.07.040.

[20] S. Shu, B.D. Wirth, P.B. Wells, D.D. Morgan, G.R. Odette, Multi-technique characterization of the precipitates in thermally aged and neutron irradiated Fe-Cu and Fe-Cu-Mn model alloys: atom probe tomography reconstruction implications, Acta Mater. 146 (2017) 237–252, https://doi.org/10.1016/j.actamat.2017.12.006.

[21] N. Almirall, P.B. Wells, H. Ke, P. Edmondson, D. Morgan, T. Yamamoto, G. R. Odette, On the elevated temperature thermal stability of nanoscale mn-ni-si precipitates formed at lower temperature in highly irradiated reactor pressure vessel steels, Sci. Rep. 9 (2019) 9587, https://doi.org/10.1038/s41598-019-45944-z.

[22] B.M. Jenkins, P.D. Styman, N. Riddle, P.A.J. Bagot, M.P. Moody, G.D.W. Smith, J. M. Hyde, Observation of Mn-Ni-Si-rich features in thermally-aged model reactor pressure vessel steels, Scr. Mater. 191 (2021) 126–130, https://doi.org/10.1016/j.scriptamat.2020.09.029.

[23] K. Lindgren, M. Boåsen, K. Stiller, P. Efsing, M. Thuvander, Cluster formation in in-service thermally aged pressurizer welds, J. Nucl. Mater. 504 (2018) 23–28, https://doi.org/10.1016/j.jnucmat.2018.03.017.

[24] B.M. Jenkins, J.O. Douglas, N. Almirall, N. Riddle, P.A.J. Bagot, J.M. Hyde, G. R. Odette, M.P. Moody, The effect of composition variations on the response of steels subjected to high fluence neutron irradiation, Materialia (Oxf) 11 (2020) 100717, https://doi.org/10.1016/j.mtla.2020.100717.

[25] K. Lindgren, M. Boåsen, K. Stiller, P. Efsing, M. Thuvander, Evolution of precipitation in reactor pressure vessel steel welds under neutron irradiation, J. Nucl. Mater. 488 (2017) 222–230, 29.

[26] F. Vurpillot, A. Bostel, D. Blavette, Trajectory overlaps and local magnification in three-dimensional atom probe, Appl. Phys. Lett. 76 (2000) 3127–3129, https://doi.org/10.1063/1.126545.

[27] A. Zakirov, Influence of the Bulk Chemical Composition on the Microstructure Evolution of Irradiated Chemically-Tailored Nuclear RPV Steels, Université de Rouen, 2022.

[28] S.V. Fedotova, E.A. Kuleshova, B.A. Gurovich, A.S. Frolov, D.A. Maltsev, G. M. Zhuchkov, I.V. Fedotov, APT-studies of phase formation features in VVER-440

RPV weld and base metal in irradiation-annealing cycles, J. Nucl. Mater. 511 (2018) 30–42, https://doi.org/10.1016/j.jnucmat.2018.08.046.
[29] B. Radiguet, P. Pareige, A. Barbu, Irradiation induced clustering in low copper or copper free ferritic model alloys, Nucl. Instrum. Methods Phys. Res. Section B 267 (2009) 1496–1499, https://doi.org/10.1016/j.nimb.2009.01.146.
[30] E. Meslin, B. Radiguet, P. Pareige, A. Barbu, Kinetic of solute clustering in neutron irradiated ferritic model alloys and a French pressure vessel steel investigated by atom probe tomography, J. Nucl. Mater. 399 (2010) 137–145, https://doi.org/10.1016/j.jnucmat.2009.11.012.
[31] F. Vurpillot, A. Bostel, E. Cadel, D. Blavette, The spatial resolution of 3D atom probe in the investigation of single-phase materials, Ultramicroscopy. 84 (2000) 213–224, https://doi.org/10.1016/S0304-3991(00)00035-8.
[32] D. Haley, T. Petersen, G. Barton, S.P. Ringer, Influence of field evaporation on radial distribution functions in atom probe tomography, Philos. Mag. 89 (2009) 925–943, https://doi.org/10.1080/14786430902821610.
[33] C. Courilleau, B. Radiguet, R. Chaouadi, E. Stergar, A. Duplessi, P. Pareige, Contributions of Ni-content and irradiation temperature to the kinetic of solute cluster formation and consequences on the hardening of VVER materials, J. Nucl. Mater. 585 (2023) 154616, https://doi.org/10.1016/j.jnucmat.2023.154616.
[34] W. Xiong, H. Ke, R. Krishnamurthy, P.B. Wells, L. Barnard, G.R. Odette, D. Morgan, Thermodynamic models of low temperature Mn-Ni-Si precipitation in reactor pressure vessel steels, Mater. Res. Soc. Commun. 4 (2014) 101–105, https://doi.org/10.1557/mrc.2014.21.
[35] K.C. Russell, L.M. Brown, A dispersion strengthening model based on differing elastic moduli applied to the iron-copper system, Acta Metallurgica 20 (1972) 969–974, https://doi.org/10.1016/0001-6160(72)90091-0.
[36] N. Castin, G. Bonny, A. Bakaev, F. Bergner, C. Courilleau, J.M. Hyde, L. Messina, G. Monnet, M.I. Pascuet, M. Serrano, L. Malerba, Multiscale modelling in nuclear ferritic steels : from nano-sized defects to embrittlement, Mater. Today Phys. 27 (2022) 1–22, https://doi.org/10.1016/j.mtphys.2022.100802.
[37] E.A. Marquis, J.M. Hyde, Applications of atom-probe tomography to the characterisation of solute behaviours, Mater. Sci. Eng.: R: Reports 69 (2010) 37–62, https://doi.org/10.1016/j.mser.2010.05.001.
[38] Y. Dong, A. Etienne, A. Frolov, S. Fedotova, K. Fujii, K. Fukuya, C. Hatzoglou, E. Kuleshova, K. Lindgren, A. London, A. Lopez, S. Lozano-perez, Y. Miyahara, Y. Nagai, K. Nishida, B. Radiguet, D.K. Schreiber, N. Soneda, M. Thuvander, T. Toyama, J. Wang, F. Sefta, P. Chou, E.A. Marquis, Atom probe tomography interlaboratory study on clustering analysis in experimental data using the maximum separation distance approach, Microsc. Microanal. (2019) 1–11, https://doi.org/10.1017/S1431927618015581.
[39] E.A. Kuleshova, S.V. Fedotova, G.M. Zhuchkov, A.D. Erak, M.A. Saltykov, M. M. Dementyeva, E.V. Alekseeva, Degradation of RPV steel structure after 45 years of operation in the VVER-440 reactor, J. Nucl. Mater. 540 (2020) 152362, https://doi.org/10.1016/j.jnucmat.2020.152362.
[40] P.D. Edmondson, C.P. Massey, M.A. Sokolov, T.M. Rosseel, An atom probe tomography study of the through wall attenuation effect on Cu-rich precipitate formation in a reactor pressure vessel steel, J. Nucl. Mater. 545 (2021) 152740, https://doi.org/10.1016/j.jnucmat.2020.152740.
[41] A. Kamboj, M.N. Bachhav, M. Dubey, N. Almirall, T. Yamamoto, E.A. Marquis, G. R. Odette, The effect of phosphorus on precipitation in irradiated reactor pressure vessel (RPV) steels, J. Nucl. Mater. 585 (2023) 154614, https://doi.org/10.1016/j.jnucmat.2023.154614.
[42] M. Carter, C. Gasparrini, J.O. Douglas, N. Riddle, L. Edwards, P.A.J. Bagot, C. D. Hardie, M.R. Wenman, M.P. Moody, On the influence of microstructure on the neutron irradiation response of HIPed SA508 steel for nuclear applications, J. Nucl. Mater. 559 (2022) 153435, https://doi.org/10.1016/j.jnucmat.2021.153435.
[43] R. Chaouadi, R. Gérard, E. Stergar, W. Van Renterghem, Neutron irradiation hardening of chemically-tailored RPV steels with respect to Cu/P and Ni/Mn elements, J. Nucl. Mater. 519 (2019) 188–204, https://doi.org/10.1016/j.jnucmat.2019.03.030.
[44] J.M. Hyde, C.A. English, An Analysis of the Structure of Irradiation induced Cu-enriched Clusters in Low and High Nickel Welds, in: Symposium R 'Microstructural Processes in Irradiated Materials, Fall MRS, 2000, https://doi.org/10.1557/PROC-650-R6.6.
[45] P.D. Styman, H. Weekes, J.M. Hyde, B. Radiguet, F. Vurpillot, G. Da Costa, C. Pareige, A. Etienne, P. Pareige, APT characterisation of radiation damage in RPV steels: experimental and data processing uncertainties, NUGENIA-PLUS: Nucl. Gener. II & III Assoc. (2016).
[46] F. De Geuser, B. Gault, Metrology of small particles and solute clusters by atom probe tomography, Acta Mater. 188 (2020) 406–415, https://doi.org/10.1016/j.actamat.2020.02.023.
[47] J.M. Hyde, G. DaCosta, C. Hatzoglou, H. Weekes, B. Radiguet, P.D. Styman, F. Vurpillot, C. Pareige, A. Etienne, G. Bonny, N. Castin, L. Malerba, P. Pareige, Analysis of radiation damage in light water reactors: comparison of cluster analysis methods for the analysis of atom probe data, Microsc. Microanal. (2017) 1–10, https://doi.org/10.1017/S1431927616012678.
[48] C. Hatzoglou, B. Radiguet, G. Da Costa, P. Pareige, M. Roussel, M. Hernandez-Mayoral, C. Pareige, Quantification of APT physical limitations on chemical composition of precipitates in Fe–Cr alloys, J. Nucl. Mater. 522 (2019) 64–73, https://doi.org/10.1016/j.jnucmat.2019.05.022.
[49] F. Vurpillot, L. Renaud, D. Blavette, A new step towards the lattice reconstruction in 3DAP, Ultramicroscopy 95 (2003) 223–229, https://doi.org/10.1016/S0304-3991(02)00320-0.
[50] F. Vurpillot, G. Da Costa, A. Menand, D. Blavette, Structural analyses in three-dimensional atom probe: a Fourier transform approach, J. Microsc. 203 (2001) 295–302, https://doi.org/10.1046/j.1365-2818.2001.00923.x.
[51] R Core Team, R: a language and environment for statistical computing, (2021). http://www.r-project.org/.
[52] D.J. Haley, posgen, (2017). https://sourceforge.net/projects/apttools/files/posgen/.
[53] A.R. Waugh, E.D. Boyes, M.J. Southon, Investigations of field evaporation with a field-desorption microscope, Surface Sci. 61 (1976) 109–142, https://doi.org/10.1016/0039-6028(76)90411-8.
[54] T.T. Tsong, G. Kellogg, Direct observation of the directional walk of single adatoms and the adatom polarizability, Phys. Rev. B 12 (1975) 1343–1353, https://doi.org/10.1103/PhysRevB.12.1343.
[55] D.J. Larson, B. Gault, B.P. Geiser, F. De Geuser, F. Vurpillot, Atom probe tomography spatial reconstruction: status and directions, Current Opinion in Solid State and, Mater. Sci. 17 (2013) 236–247, https://doi.org/10.1016/j.cossms.2013.09.002.
[56] R. Lawitzki, P. Stender, G. Schmitz, Compensating local magnifications in atom probe tomography for accurate analysis of nano-sized precipitates, Microsc. Microanal. 27 (2021) 499–510, https://doi.org/10.1017/S1431927621000180.
[57] N. Rolland, F. Vurpillot, S. Duguay, D. Blavette, A. Meshless, Algorithm to model field evaporation in atom probe tomography, Microsc. Microanal. 21 (2015) 1649–1656, https://doi.org/10.1017/S1431927615015184.
[58] B. Klaes, R. Lardé, F. Delaroche, S. Parviainen, N. Rolland, S. Katnagallu, B. Gault, F. Vurpillot, A model to predict image formation in the three-dimensional field ion microscope, Comput. Phys. Commun. 260 (2021) 107317, https://doi.org/10.1016/j.cpc.2020.107317.
[59] D.R. Kingham, The post-ionization of field evaporated ions: a theoretical explanation of multiple charge states, Surf. Sci. 116 (1982) 273–301, https://doi.org/10.1016/0039-6028(82)90434-4.
[60] R. Dubosq, B. Gault, C. Hatzoglou, K. Schweinar, F. Vurpillot, A. Rogowitz, G. Rantitsch, D.A. Schneider, Analysis of nanoscale fluid inclusions in geomaterials by atom probe tomography: experiments and numerical simulations, Ultramicroscopy. 218 (2020) 113092, https://doi.org/10.1016/j.ultramic.2020.113092.
[61] C. Hatzoglou, B. Klaes, F. Delaroche, G.D. Costa, B. Geiser, M. Kühbach, P.B. Wells, F. Vurpillot, Mesoscopic modeling of field evaporation on atom probe tomography, J. Phys. D: Appl. Phys. 56 (2023) 375301, https://doi.org/10.1088/1361-6463/acd649.
[62] H. Ke, P.B. Wells, P.D. Edmondson, N. Almirall, L. Barnard, G.R. Odette, D. Morgan, Thermodynamic and kinetic modeling of Mn-Ni-Si precipitates in low-Cu reactor pressure vessel steels, Acta Materialia Submitted (2017) 10–26, https://doi.org/10.1016/j.actamat.2017.07.021.
[63] P. Bas, A. Bostel, B. Deconihout, D. Blavette, A general protocol for the reconstruction of 3D atom probe data, Appl. Surf. Sci. 87–88 (1995) 298–304, https://doi.org/10.1016/0169-4332(94)00561-3.
[64] E.A. Marquis, V.J. Araullo-Peters, Y. Dong, A. Etienne, S.V. Fedotova, K. Fujii, K. Fukuya, E.A. Kuleshova, A. Lopez, A.J. London, S. Lozano-Perez, Y. Nagai, K. Nishida, B. Radiguet, D. Schreiber, N. Soneda, M. Thuvander, T. Toyama, F. Sefta, P. Chou, On the use of density-based algorithms for the analysis of solute clustering in atom probe tomography data, in: Proceedings of the 18th International Conference on Environmental Degradation of Materials in Nuclear Power Systems – Water Reactors. The Minerals, Metals & Materials Series., 2019. https://doi.org/10.1007/978-3-030-04639-2_141.
[65] J.M. Hyde, M.G. Burke, B. Gault, D.W. Saxey, P.D. Styman, K.B. Wilford, T. J. Williams, Atom probe tomography of reactor pressure vessel steels: an analysis of data integrity, Ultramicroscopy. 111 (2011) 676–682, https://doi.org/10.1016/j.ultramic.2010.12.033.
[66] A. Cerezo, T.J. Godfrey, S.J. Sijbrandij, G.D.W. Smith, P.J. Warren, Performance of an energy-compensated three-dimensional atom probe, Rev. Scientif. Instrum. 69 (1998) 49–58, https://doi.org/10.1063/1.1148477.
[67] M.P. Moody, B. Gault, L.T. Stephenson, D. Haley, S.P. Ringer, Qualification of the tomographic reconstruction in atom probe by advanced spatial distribution map techniques, Ultramicroscopy. 109 (2009) 815–824, https://doi.org/10.1016/j.ultramic.2009.03.016.
[68] D. Blavette, I. Blum, F. Cuvilly, G. Da Costa, F. Danoix, J. Houard, W. Lefebvre-Ulrikson, C. Pareige, L. Rigutti, X. Sauvage, A. Vella, F. Vurpillot, Atom Probe tomography: Put Theory Into Practice, Academic Press, an imprint of Elsevier, Amsterdam Boston Heidelberg, 2016.
[69] B. Gault, M.P. Moody, F. De Geuser, A. La Fontaine, L.T. Stephenson, D. Haley, S. P. Ringer, Spatial resolution in atom probe tomography, Microsc. Microanal. 16 (2010) 99–110, https://doi.org/10.1017/S1431927609991267.
[70] G.R. Odette, T. Yamamoto, T.J. Williams, R.K. Nanstad, C.A. English, On the history and status of reactor pressure vessel steel ductile to brittle transition temperature shift prediction models, J. Nucl. Mater. 526 (2019) 151863, https://doi.org/10.1016/j.jnucmat.2019.151863.
[71] P. Kluṕś, D. Haley, A.J. London, H. Gardner, J. Famelton, B.M. Jenkins, J.M. Hyde, P.A.J. Bagot, M.P. Moody, PosgenPy: an automated and reproducible approach to assessing the validity of cluster search parameters in atom probe tomography datasets, Microsc. Microanal. (2021) 1–10, https://doi.org/10.1017/s1431927621012368.